Paper-supported 3D cell culture for tissue-based bioassays

Ratmir Derda[a,b], Anna Laromaine[a], Akiko Mammoto[c], Sindy K. Y. Tang[a], Tadanori Mammoto[c], Donald E. Ingber[b,c,d], and George M. Whitesides[a,b,1]

[a]Department of Chemistry and Chemical Biology, [b]Wyss Institute for Biologically Inspired Engineering, and [d]School of Engineering and Applied Sciences, Harvard University, Cambridge, MA 02138; and [c]Vascular Biology Program, Departments of Pathology and Surgery, Children's Hospital and Harvard Medical School, Boston, MA 02115

Contributed by George M. Whitesides, September 17, 2009 (sent for review August 19, 2009)

Fundamental investigations of human biology, and the development of therapeutics, commonly rely on 2D cell-culture systems that do not accurately recapitulate the structure, function, or physiology of living tissues. Systems for 3D cultures exist but do not replicate the spatial distributions of oxygen, metabolites, and signaling molecules found in tissues. Microfabrication can create architecturally complex scaffolds for 3D cell cultures that circumvent some of these limitations; unfortunately, these approaches require instrumentation not commonly available in biology laboratories. Here we report that stacking and destacking layers of paper impregnated with suspensions of cells in extracellular matrix hydrogel makes it possible to control oxygen and nutrient gradients in 3D and to analyze molecular and genetic responses. Stacking assembles the ''tissue'', whereas destacking disassembles it, and allows its analysis. Breast cancer cells cultured within stacks of layered paper recapitulate behaviors observed both in 3D tumor spheroids in vitro and in tumors in vivo: Proliferating cells in the stacks localize in an outer layer a few hundreds of microns thick, and growth-arrested, apoptotic, and necrotic cells concentrate in the hypoxic core where hypoxia-sensitive genes are overexpressed. Altering gas permeability at the ends of stacks controlled the gradient in the concentration of the O_2 and was sufficient by itself to determine the distribution of viable cells in 3D. Cell cultures in stacked, paper-supported gels offer a uniquely flexible approach to study cell responses to 3D molecular gradients and to mimic tissue- and organ-level functions.

diffusion | hypoxia | molecular gradients | multilayer constructs

A distinguishing feature of cell growth in 3D is the diffusion-limited distribution of oxygen, nutrients, metabolites, and signaling molecules, which are continuously consumed and produced by the cells (1, 2). These distributions are not mimicked in 2D monolayer cultures (3–5). Chemical gradients influence embryo development, tissue homeostasis, and pathologies ranging from cancer to infectious disease. The mass transport of oxygen and nutrients is particularly important because it limits cell proliferation in 3D cultures to distances less than a few hundred microns from convectively stirred, oxygenated medium (2, 6) or in living tissues to similar distance from capillary blood vessels (7, 8). Validating mechanisms for regulation of cell growth in 3D requires culture systems in which gradients can be designed, generated, and tested (6). Chemical gradients in tissues are often generated by cellular metabolism. Hence, controlling the distribution of oxygen and nutrients in 3D cultures is only possible if the location and properties of cells can be manipulated on a scale similar to the characteristic length that balances diffusion and metabolism (hundreds of microns) in tissue. Methods that enable generation and analysis of such distributions in vivo (e.g., tissue-specific gene expression, laser microdissection) or in vitro [e.g., studies in microfabricated devices (9–12)] exist, but are time consuming to use and require specialized engineering approaches or instrumentation not available in most biology laboratories.

In this report, we present a strategy for controlling the distribution of cultured cells in 3D by fabrication of multilaminate structures of fiber-supported hydrogels with each layer composed of chromatography paper impregnated with an extracellular matrix (ECM) hydrogel containing living cells. This technique starts by adding a hydrogel precursor, as a fluid containing suspended cells, to a paper support and gelling it in place. This simple procedure generates 3D fiber-supported gels with defined numbers and densities of cells with easily controlled lateral dimensions and with thickness defined by the paper. Importantly, a single layer (SL) of paper impregnated with the hydrogel containing cells is sufficiently strong mechanically that it can be easily manipulated and stacked into multiple-layer constructs to generate 3D cultures. These constructs control the properties of 3D cultures of cells at the $n \times 100$-μm length scale that is relevant to mass transport in vivo. We demonstrate that these constructs may be designed to exhibit desired spatial distributions of cells, and they can be easily destacked to analyze cell structure and function within physical sections of these 3D tissues structures without requiring optical or histological sectioning.

Results

Analysis of Cells Inside Paper Permeated with Hydrogels. When a suspension of cells in a hydrogel precursor (liquid) is placed in contact with dry paper, the fluid containing the cell redistributes by capillary wicking, and the cells are carried with the flow of liquid. To analyze geometry of the 3D culture generated in this process, we spotted suspension of HS-5 cells stably expressing mCherry fluorescent protein in Alexa Fluor 488-labeled Matrigel on 200 μm-thick chromatography paper (Fig. 1*A*). The use of solutions containing different concentrations of cells (1.3×10^6–4×10^7 cells/mL) made the variance of concentration of cells in 3D cultures straightforward. Spotting different volumes of cell suspension onto the paper (1–5 μL) changed the area of these 3D cultures (Fig. 1 *B*–*D*). We incubated the samples in growth media for four hours, fixed them, and stained them with Alexa Fluor 633-conjugated phalloidin to label intracellular F-actin. A fluorescent gel scanner showed the distribution of cells (Fig. 1*B*) and matrix (Fig. 1*C*) in the resulting constructs; as expected, the area of a 3D culture that contains cells within a paper is similar to the area of spreading of liquid hydrogel precursor (Fig. 1*E*).

To quantify the number of cells inside the paper, in the images obtained by fluorescent gel scanner we defined the background intensity as that of the paper that did not contain any cells and

Author contributions: R.D., A.L., A.M., D.E.I., and G.M.W. designed research; R.D., A.L., A.M., and T.M. performed research; S.K.Y.T. contributed new reagents/analytic tools; R.D., A.L., A.M., and T.M. analyzed data; and R.D., D.E.I., and G.M.W. wrote the paper.

The authors declare no conflict of interest.

[1]To whom correspondence should be addressed. E-mail: gwhitesides@gmwgroup.harvard.edu.

This article contains supporting information online at www.pnas.org/cgi/content/full/0910666106/DCSupplemental.

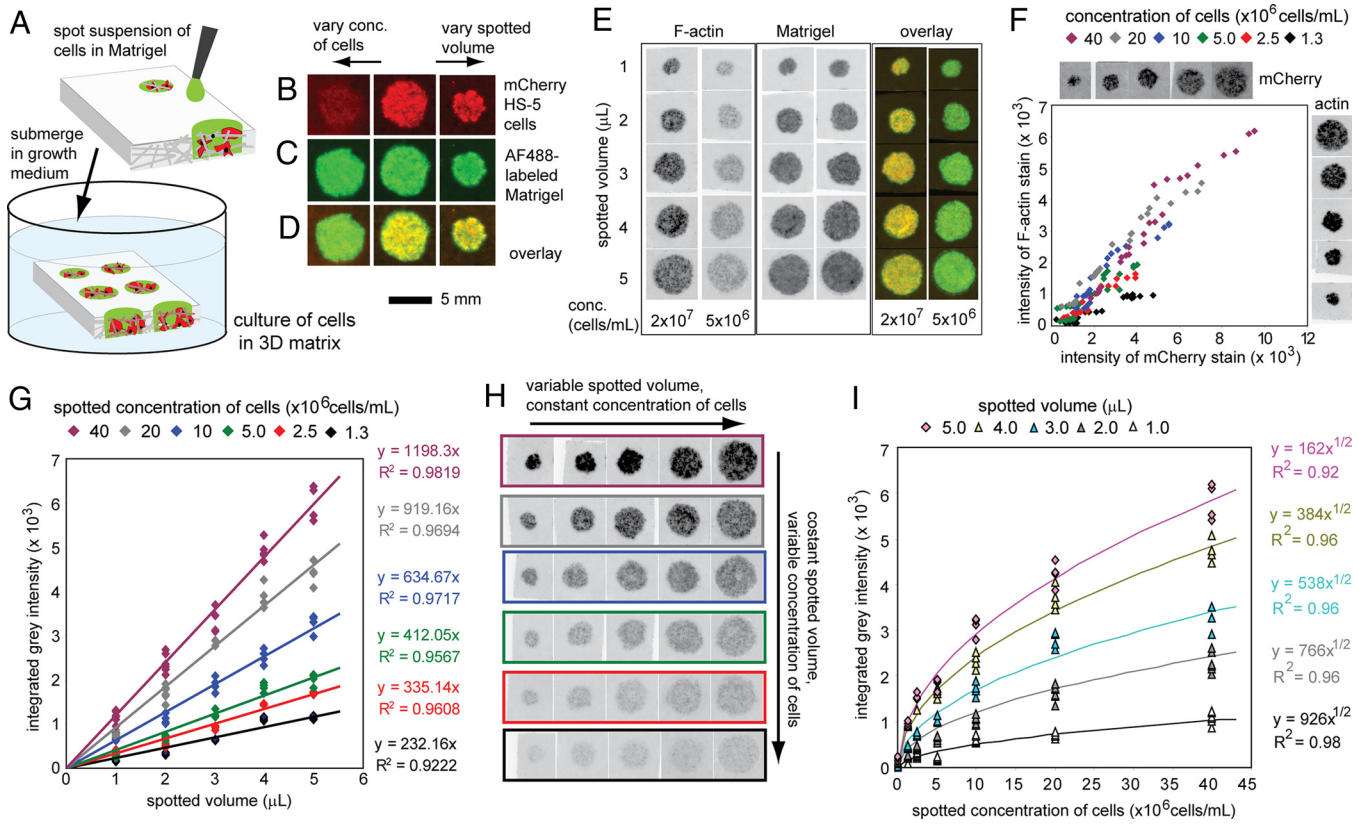

Fig. 1. Generation and characterization of 3D cultures of defined physical dimensions. (*A*) Permeation of Matrigel or other hydrogel precursors into chromatography or filter paper yields paper-supported hydrogels of thickness akin to that of the paper and lateral dimensions determined by the volume spotted. (*B*—*D*) Spotting of a suspension of mCherry-HS5 cells in cold (4 °C) Matrigel labeled with AF488, followed by immersion in 37° C media, led to gelation of Matrigel inside the paper. Using a different volume of spotted solution controlled the spotted area. Using different concentrations of cells controlled the number of cells per spotted area. Imaging with a fluorescent gel scanner visualized cells (*B*), matrix (*C*), and their colocalization (*D*) inside paper. (*E*) The area that contains HS-5 cells within a paper is similar to the area of spreading of Matrigel. (*F*) Integrated fluorescent intensity of endogenous mCherry fluorescence correlated linearly with fluorescence of F-actin stain. (*G*–*I*) We measured the integrated fluorescent intensity of 3D cultures and interpolated the intensity as a function of area (*G*) and cell density (*I*) ($n = 4$ for each size and concentration; all data are presented). Representative images of each culture are presented in *H*.

measured integrated gray-scale intensity above this background. F-actin and mCherry fluorescence were linearly correlated; F-actin can thus be used to quantify the cells in paper-supported 3D matrices (Fig. 1*G*). The integrated fluorescent intensity in samples that presented 3D cultures of different area also correlated linearly with that area (Fig. 1*H*). We further quantified 3D cultures of equal areas that presented different densities of cells. The integrated fluorescence of the samples is a nonlinear function of the density of HS-5 cells (Fig. 1*H*). The dependence for other types of cells (human breast cancer cells, MDA-MB-231) and other types of dyes that bind F-actin was similar (Fig. S1). The observed dependence—fluorescence vs. (concentration)$^{1/2}$—is similar to that of fluorescent dyes trapped in paper and other thick scattering media (13), and it can be used, for example, to quantify proliferation of cells in paper-supported hydrogels (Fig. S1).

Stacking of Cell-Containing Constructs Controls the Geometry and Behavior of Cells in 3D Cultures. Stacking and destacking of cell-containing constructs makes it possible to manipulate gradients of soluble molecules in these constructs and to characterize cells in these complex gradients; all would be challenging or impossible in conventional 3D cultures based on hydrogels, cell spheroids, or 3D perfusion reactors (12, 14). To create a 3D structure with dimensions relevant to mass transport of oxygen and glucose, we stacked eight 200-μm-thick layers of paper (L1–L8), each containing the same density of MDA-MB-231 cells (Fig. 2*A* and Fig. S1). This stacked 3D culture is automatically equipped (by virtue of its method of fabrication) with a built-in ruler. For example, cells in the first layer (L1) are 0–200 μm from convectively stirred medium, and those in L5–L8 are 1,000–1,600 μm from this medium. After nine days of culturing, we destacked the eight layers. The number of cells in layers L5–L8 was the same as the initial number of cells plated in these layers (red line in Fig. 2*B*). The number of cells in the top layer L1 was, however, significantly higher than the initial number of cells (Fig. 2 *B* and *C*), and proliferation of cells in layer L1 was similar to that in a separate, 200-μm-thick SL of paper (Fig. S1). Suppression of cell growth in layers L5–L8 was independently confirmed by the finding that these cells also contained significantly lower levels of S-phase entry and higher levels of DNA damage than cells in the layers L1 or SL (Fig. 2 *D* and *E*).

The behavior of cells in the eight-layer stack recapitulates that observed in 3D tumor spheroids (5, 6), with proliferating cells located in an outer layer (hundreds of microns in thickness) and growth-arrested, apoptotic, or necrotic cells concentrated in a hypoxic core. Unlike tumor spheroids, many cell types can be incorporated in multilayer cultures. Distributions of cells in these layers differ according to the types of cells (Fig. S2) because types of cells differ in their rates of metabolism and resistance to deprivation of oxygen and nutrients. Within these distributions, cells exhibit physiological and morphological changes in response to molecular gradients. For example, the size of lumens formed by endothelial cells in a multilayer stack depends on the

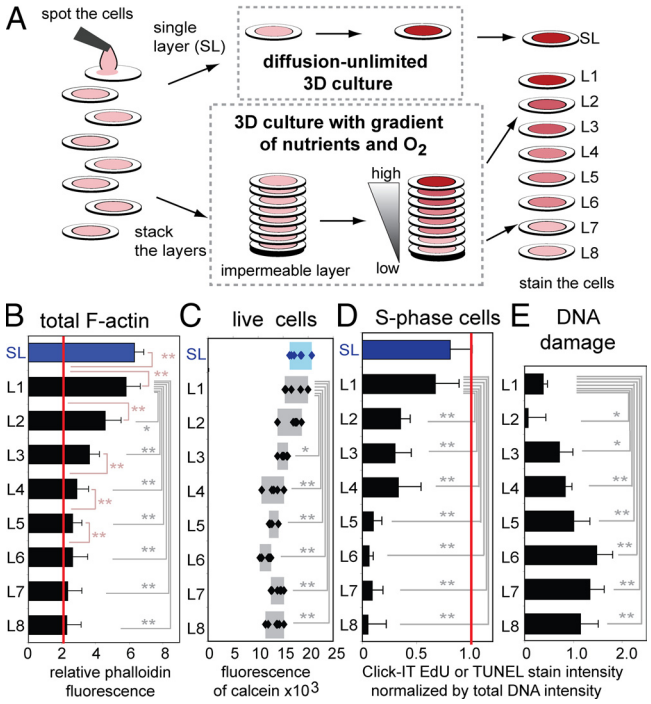

Fig. 2. Properties of cells after nine days of culture in thick (1,600 μm) 3D cultures made of multiple stacked layers of paper (L1–L8) and comparison with thin 3D cultures comprising a SL of paper. (*A*) Schematic of the plating, culture and analysis. In *B–E*, samples were cultured for nine days and fixed. Separated layers were stained with AF633-phalloidin ($n = 12$) (*B*), Click-It EdU kit ($n = 8$) (*D*), Click-It TUNEL kit ($n = 8$) (*E*); in *C*, separated layers were incubated with calcein solution for 20 min and fixed ($n = 6$). Intensities of the stains in *B–E* were normalized to those obtained in SL samples after one day of culture (vertical red line). For $n > 7$, the average and an error bar equal to one standard deviation are presented. For $n < 7$, all data are presented (the box highlights the range of data). *, $P < 0.05$; **, $P < 0.01$.

distance of these cells from oxygenated culture medium (Fig. S2 *I–N*) (15).

Destacking of Multilayered Constructs Permits Simple Isolation of Viable Cells from Defined Locations in 3D. Isolation of cells (in thin cell-containing slices) from 3D tissue constructs is critical for the cells' biochemical and genetic characterization. Destacking of multilayered cultures eliminates the need for histological sectioning, cell sorting (16), or other manipulations that take time, perturb 3D architecture, and compromise cell viability. For example, a standard method for quantification of viable cells involves measuring rates of turnover of metabolic probes (Fig. S1); such measurements are challenging in thick 3D cultures, because reagent diffusion competes with reagent turnover (Fig. S3). Destacking the layers minimizes the influence of diffusion (Fig. S3). Thus, by measuring the turnover rate of Alamar Blue reagent in destacked layers, we confirmed that the number of cells in layers L5–L8 after nine days of culture was similar to the number originally plated (40,000 per layer, red line in Fig. 3*B*), whereas the number of cells in layer L1 or SL increased by factors of 3–4. After destacking, we monitored the cells isolated from different locations in these 3D cultures. Four days after separation of the layers, the number of viable cells in all layers increased. Cells in growth-limited locations of 3D culture are, therefore, capable of resuming proliferation once exposed to normal concentration of oxygen and nutrients (Fig. 3 *C* and *D*). It would be impossible to measure the proliferation of cells without physical isolation of viable sections of the 3D cultures.

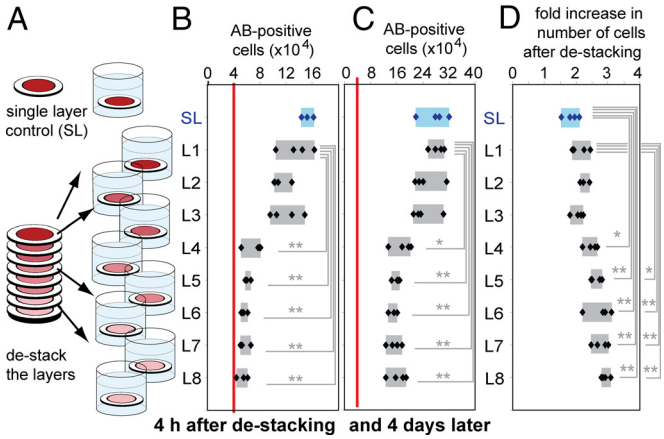

Fig. 3. Isolation of viable cells from defined areas of 3D culture. In *A*, samples were cultured in stacks for nine days, destacked, and placed in separated wells containing Alamar Blue. (*B* and *C*) The rate of substrate turnover determined the number of cells four hours (*B*) or four days (*C*) after destacking ($n = 4$). (*D*) The ratio of values from *B* and *C*. All data are presented (the box highlights the range of data). *, $P < 0.05$; **, $P < 0.01$.

Oxygen Gradients Regulate Distribution of Cells in Multilayered 3D Constructs. To determine whether the observed responses are governed by gradients in nutrients or oxygen, or by gradients in other factors (for example, pH or metabolites), we analyzed changes in the expression of oxygen-responsive genes (17) by destacking the layers and isolating RNA from cells originally located at different distances from the culture medium (Fig. 4*A*). The cells in the layers furthest from the bulk media had the highest level of expression of VEGF and IGFBP3—both markers of hypoxia (Fig. 4*B*). As a control, we tested the eight-layer stack under conditions that allowed perfusion of the medium into its center from the sides, and precluded establishing a stable gradient of nutrients or oxygen (Fig. 4*C*). Cells cultured in these "loosely packed layers" did not show a gradient of expression of VEGF and IGFPB3 (Fig. 4*D*). Distribution of S-phase cells was also equal in these layers (Fig. 4*E*).

We further decoupled the mass transport of oxygen from that of soluble nutrients by replacing the impermeable cellulose acetate layer beneath L8 with a 1-mm-thick layer of poly(dimethylsiloxane (PDMS) (Fig. 5*A*). PDMS is impermeable to water, protons and glucose, but very permeable to oxygen and carbon dioxide (18). Analysis of an eight-layer stack after destacking showed that there was no significant difference in the numbers of viable cells in layer L1 (which was in contact with medium) and L8 (which was in contact with PDMS) (Fig. 5 *B–D*), but that layers L3 and L4 (middle of the stack) had lower numbers of cells than either end. Regulation of the gradients in concentration of oxygen thus demonstrated that diffusion of oxygen to the cells, but not of soluble nutrients or protons (19), is the major determinant of cell survival in these 3D cultures (Fig. 5 *E* and *F*).

Analysis of Distribution of Cells in Multilayered Constructs in Vivo. We implanted multilayer stacks of paper containing Lewis lung carcinoma (LLC) cells (Fig. S4) s.c. in the backs of C57BL mice (Fig. 6 and Fig. S4). After three days, the distribution of cells in isolated layers (SL or in the L1–L8 layers) in vivo (Fig. 6 *B*, *F*, and *G*) resembled that observed in analogous constructs cultured in vitro (Fig. 6 *A*, *C–E*). In contrast to in vitro cultures, layers adjacent to the tissue also contained cells invading from surrounding tissues that displayed markers of differentiated hematopoietic cells (CD45), and endothelial cells (CD31) (Fig. 6 *J–P* and Fig. S4). Neovascularization of these tumor implants

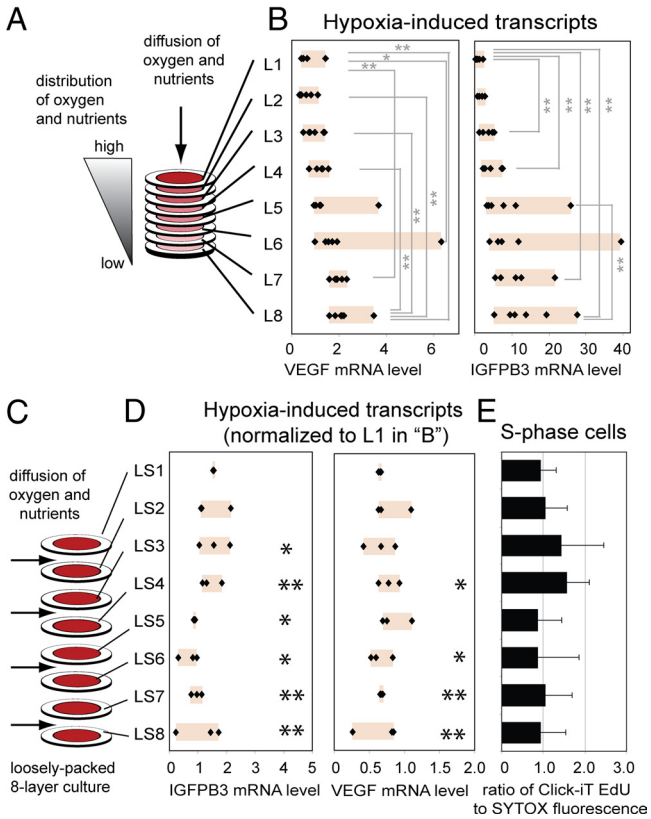

Fig. 4. Expression levels of oxygen-responsive genes in different locations of 3D culture. (*A* and *B*) Real-time PCR-quantified levels of expression of VEGF and IGFBP3 transcripts using $\Delta\Delta C_t$ values relative to beta-2 microglobulin and reported as ''fold increase'' with respect to L1 samples ($n = 6$). (*C–E*) In the loosely packed eight-layer stack, no gradient of expression of VEGF and IGFPB3 was observed ($n = 3$) (*D*), and the fraction of S-phase cells is the same in all layers LS1–LS8 ($n = 8$) (*E*). In *D*, RNA levels in LS1–LS8 are normalized to those of L1 in *B* and were significantly different from the corresponding layers L1–L8. All data are presented (the box highlights the range of data). *, $P < 0.05$; **, $P < 0.01$.

was also confirmed by injecting fluorescently labeled Con A (ConA) intravenously and observing labeled capillaries at the periphery of the constructs (Fig. 4 *M–P* and Fig. S4). Thus, this 3D culture system, based on stacked paper, permits investigation of the responses of cells to molecular gradients in vivo.

Discussion

The combination of paper and hydrogels provides a versatile and experimentally convenient solution to the problem of creating 3D, gel-based structures of defined geometry for the growth of cells. Because paper is simultaneously thin (<200 μm), mechanically strong, and a largely (60–80%) void space, the cells in the paper-supported hydrogels are not limited by mass transport in their access to nutrients and oxygen, or in their loss of metabolic by-products. In this report, we used chromatography paper which is 200 μm thick. Paper of other types, however, can be used to create paper-supported hydrogels of thickness ranging from 30 μm (lens paper) to 1,500 μm (blotting paper). Aside from Matrigel, other temperature-responsive gels—such as collagen, and hydrogels responsive to pH, ionic strength, polyvalent ions, or other stimuli to gellation—could be used.

Multilayered 3D constructs allow the combination of different types of cells, and cells in multiple 3D geometries, to create structured, heterogeneous 3D cultures both in vitro and in vivo. Gradients in concentration of oxygen, metabolites, and other molecules that are consumed or produced by cells (e.g., signaling molecules, drugs) are spontaneously generated in these multilayered constructs. The ability to destack these 3D constructs into SLs that contain live cells, and to analyze each layer individually, provides a simple process to use when carrying out biochemical and genetic analyses of tissue sections in these gradients without the requirement that cells be fixed, freezed, or sorted. These capabilities can be broadly useful in cell-based high-throughput screening and drug discovery because multilayered 3D constructs can be integrated easily with most cell-based assays and high-throughput screens. Multiple layers of paper can be incorporated into standard microwell plates, for example, by assembling multiple layers of paper, 96-zone plates (20), and commercially available bottomless 96-well plates. In addition, strategies for synthesis of chemical libraries on paper are well developed (21, 22), and this technology can be combined with multilayer cell culture to provide screening assays (23).

Implantation and subsequent isolation of viable multilayer 3D constructs provides a simple approach to the investigation of spatially dynamic cell growth in materials in vivo and for modeling molecular gradients of metabolites, signaling molecules, or drugs in nonvascularized tissues. We observed that patterns of cell survival in multilayered constructs in vivo are similar, but not identical, to those in analogous constructs in vitro. Investigation of the differences between the two cultures can be used for systematic comparison and optimization of 3D culture conditions in vitro and to mimic conditions encountered in vivo. A steeper ''survival gradient'' in vivo (Fig. 6 *A* and *B*) may arise from differences in the balance of reaction and diffusion: cells infiltrating from the tissue into the construct deplete nutrients and oxygen. The boundary conditions, i.e., the concentration of oxygen and nutrients at the contact with tissue and medium, are also different. The ability to alter the permeability of individual layers and of a stack (Fig. 5) and to block the infiltration of cells or the diffusion of specific components can be used to dissect these variables. The differences, however, may also arise from intrinsic differences in LLC cells exerted by in vitro and in vivo extracellular environments. The ability to isolate individual layers containing minimally perturbed viable cells (Fig. 3) can be used to investigate (*i*) these differences by systematically comparing physiologies of cells from different environments, and (*ii*) profiling by using biochemical and genomic approaches. We believe that the gradient we detect in vitro will resemble those encountered by cells in the more-complex in vivo environment.

We propose that 3D matrices comprising stacked layers of paper (or other fibrous or porous materials) supporting hydrogels that contain cells will provide a broadly useful, versatile tool with which to explore areas of fundamental cell biology, tissue engineering, and drug development.

Methods

For the hydrogel, we used basement-membrane extract from Engelbreth–Holm–Swarm sarcoma (Matrigel). This hydrogel is a liquid at 4 °C, and rapidly gels above 10 °C (24). We spotted suspension of cells (10^7 cells/mL unless otherwise mentioned) in Matrigel at 4 °C onto 200-μm-thick chromatography paper; immersion of the gel-paper composite in warm culture medium (25–35 °C) yielded a structure with the thickness and mechanical strength of wet paper and with lateral dimensions (2–8 mm) defined by the volume of liquid used in spotting (1–5 μL). Because cells are plated in 4 °C cold matrix, before any assay we equilibrated the samples in 36 °C warm culture medium for 24 h to allow the cells to recover from the effects of short-term exposure to cold and decrease in cellular metabolism (Fig. S5). To create multilayered cultures, we stacked cell-containing papers on top of a film of cellulose acetate (which is impermeable to both O_2 and water) or PDMS (which is permeable to O_2 but impermeable to water) and gripped the layers with a custom-made holder. All handling was performed manually by using sterile tweezers. We cultured papers submerged in dishes filled with growth media agitated at 40 rpm in 36 °C, 5% CO_2 incubator. We stained papers with solutions of Alexa Fluor-conjugated phalloidin, Click-It EdU, Click-It TUNEL, SYTOX green, propidium

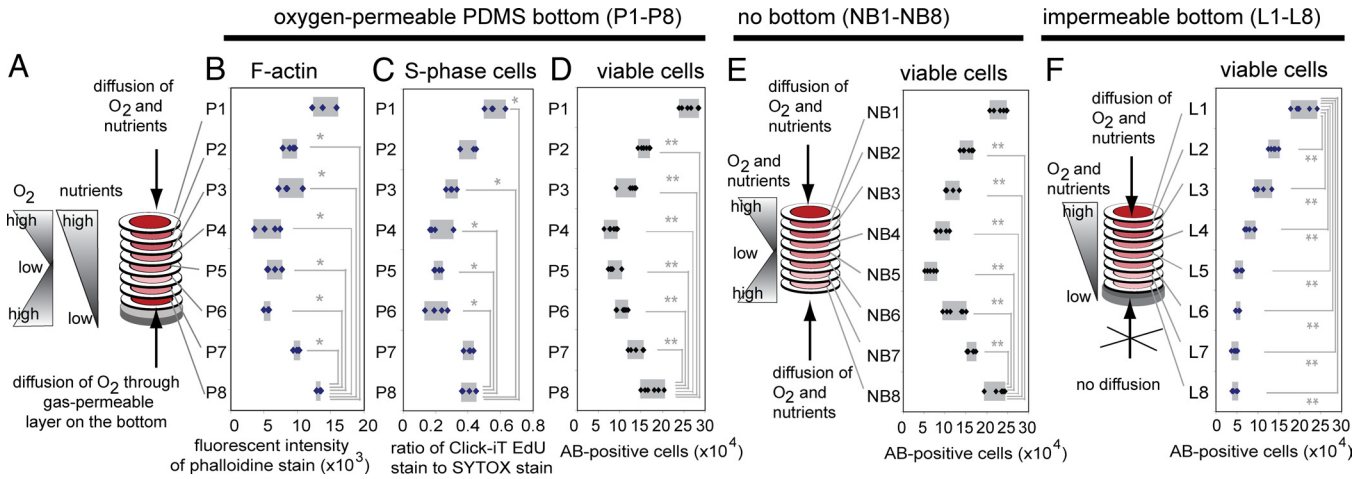

Fig. 5. Changing gas permeability of the terminal layers reveals that the distribution of cells in 3D follows that of O_2. (*A–D*) When a PDMS layer was placed on the bottom of the closely packed eight-layer stack (P1–P8), oxygen could access the bottom (P8) layers; the number of cells ($n = 4$) and the number of S-phase cells ($n = 4$) (*C*) in the bottom layers (P8) was significantly higher than in the middle layers (e.g., P4), although it was lower than in the layer exposed to culture media (P1). (*D–F*) The number of viable cells in stacks containing a bottom layer made of PDMS (*D*), cellulose acetate (*F*), or no layer at all (*E*) was determined by using Alamar Blue ($n = 6$ in *E* and *F*). All data are presented (the box highlights the range of data). *, $P < 0.05$; **, $P < 0.01$.

iodide, or calcein and imaged by using a fluorescent gel scanner or a confocal microscope. Long-term metabolic activity was monitored by sampling growth media containing Alamar Blue and comparing the rate of substrate turnover to the calibration curve (Fig. S1). Data were compared by using the rank-sum Wilkinson test; numbers of replicates and alpha values are indicated in the figure legends. Details of cell culture, metabolic assays, in vivo assay, staining, and biochemical procedures are described in the *Materials and Methods* section of the *SI Text*.

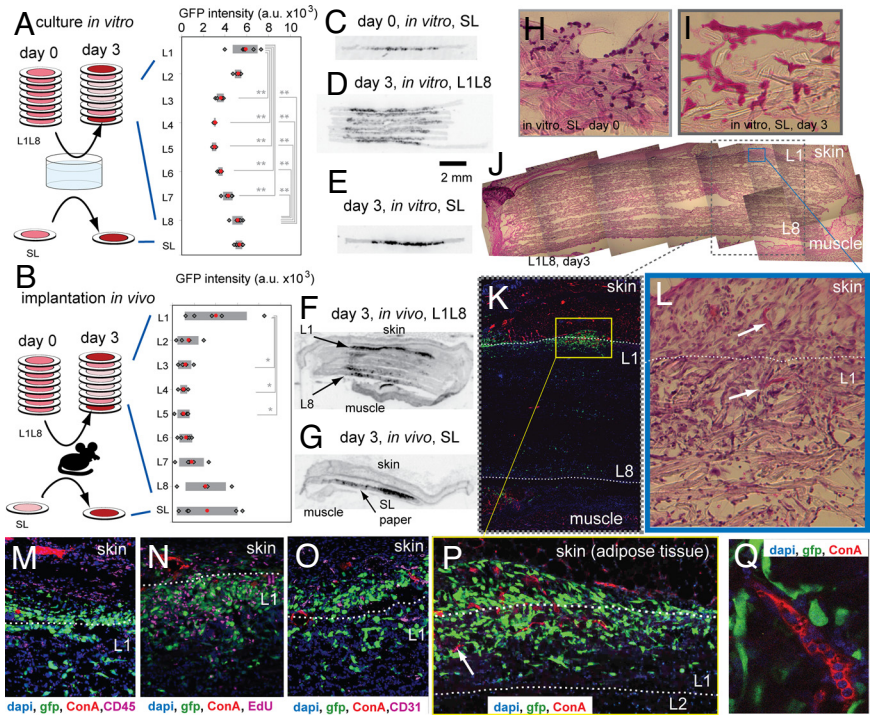

Fig. 6. Comparison of distribution of cells in multilayer stacks in vivo and in vitro. (*A* and *B*) We cultured LLC-GFP cells in SL and multilayer (L1-L8) constructs for three days in vitro ($n = 6$) (*A*) or implanted these constructs s.c. in C57BL mice ($n = 5$) (*B*), isolated the layers, and measured GFP fluorescence in every layer. The number of cells in SL and terminal layers (L1 or L8) was significantly higher than that in the middle layers. All data are presented; the overlaid box is centered on the average value, and its width is twice the standard deviation. *, $P < 0.05$; **, $P < 0.01$. (*C–G*) We also analyzed the distribution of cells by sectioning the SL and multilayer (L1–L8) samples from culture in vitro (*C–E*) and in vivo (*F–G*). We imaged the sections by using a gel scanner; representative images show inverse intensity of the green fluorescence. (*H* and *I*) Hematoxylin and eosin (HE) staining of the 18-μm-thick sections of the samples immediately after plating (*H*), and after three days of culture in vitro (*I*). (*J–P*) HE-staining and immunofluorescent staining of 18-μm-thick sections of multilayer constructs cultured in vitro confirm that GFP-LLC cells (green in all images) reside in terminal layers and also infiltrate the adjacent tissue. Frames *K–P* demonstrate distribution of CD45(+) cells (*M*), S-phase cells (*N*), CD31(+) cells (*O*), and functional capillaries (red in *M–P*, white arrows in *P* and *L*) stained by i.v. injection of rhodamine-ConA. (*Q*) High-magnification image of the capillary inside the L1 layer. We acquired images by using confocal (*I*, *M–P*) or dissecting (*H–K*) microscopes with 4×, 10×, 20×, or 67× objective. Blue, DAPI; green, GFP; red, rhodamine-ConA; purple, CD31 (*M*), EdU (*N*), CD45 (*O*).

ACKNOWLEDGMENTS. We thank Estrella Lee for assistance with cell culture, Dr. Martin Montoya–Zavala for assistance with confocal microscopy, and Professor Emanuel Carrilho for assistance with patterning of paper. We are grateful to the Kenneth Anderson Lab (Dana–Farber Cancer Institute, Boston) for providing the HS-5 cell line, and Lois E. H. Smith's (Children's Hospital, Boston) lab for the use of automated microscopes. This work was supported by funds from Vertex Inc., the Wyss Institute of Biologically Inspired Engineering, Fulbright-Generalitat de Catalunya (to A.L.), the American Heart Association (to A.M.), and by National Insitutes of Health Grant ES 016665 (to G.M.W.), and a Department of Defense Breast Cancer Innovator Award (to D.E.I.).

1. Minchinton AI, Tannock IF (2006) Drug penetration in solid tumours. *Nat Rev Cancer* 6:583–592.
2. Malda J, Klein TJ, Upton Z (2007) The roles of hypoxia in the In vitro engineering of tissues. *Tissue Eng Part A* 13:2153–2162.
3. Yamada KM, Cukierman E (2007) Modeling tissue morphogenesis and cancer in 3D. *Cell* 130:601–610.
4. Schmeichel KL, Bissell MJ (2003) Modeling tissue-specific signaling and organ function in three dimensions. *J Cell Sci* 116:2377–2388.
5. Pampaloni F, Reynaud EG, Stelzer EHK (2007) The third dimension bridges the gap between cell culture and live tissue. *Nat Rev Mol Cell Biol* 8:839–845.
6. Folkman J, Hochberg M (1973) Self-regulation of growth in 3 dimensions. *J Exp Med* 138:745–753.
7. Thomlinson RH, Gray LH (1955) The histological structure of some human lung cancers and the possible implications for radiotherapy. *Br J Cancer* 9:539–549.
8. Vaupel P, Kallinowski F, Okunieff P (1989) Blood-flow, oxygen and nutrient supply, and metabolic microenvironment of human-tumors—a review. *Cancer Res* 49:6449–6465.
9. McGuigan AP, Sefton MV (2006) Vascularized organoid engineered by modular assembly enables blood perfusion. *Proc Natl Acad Sci USA* 103:11461–11466.
10. Nelson CM, Inman JL, Bissell MJ (2008) Three-dimensional lithographically defined organotypic tissue arrays for quantitative analysis of morphogenesis and neoplastic progression. *Nat Protoc* 3:674–678.
11. Albrecht DR, Underhill GH, Wassermann TB, Sah RL, Bhatia SN (2006) Probing the role of multicellular organization in three-dimensional microenvironments. *Nat Methods* 3:369–375.
12. Griffith LG, Swartz MA (2006) Capturing complex 3D tissue physiology in vitro. *Nat Rev Mol Cell Biol* 7:211–224.
13. Ferreira LFV, Freixo MR, Garcia AR, Wilkinson F (1992) Photochemistry on surfaces—fluorescence emission quantum yield evaluation of dyes adsorbed on microcrystalline cellulose. *J Chem Soc Faraday Trans* 88:15–22.
14. Martin Y, Vermette P (2005) Bioreactors for tissue mass culture: Design, characterization, and recent advances. *Biomaterials* 26:7481–7503.
15. Eguchi R, Suzuki A, Miyakaze S, Kaji K, Ohta T (2007) Hypoxia induces apoptosis of HUVECs in an in vitro capillary model by activating proapoptotic signal p38 through suppression of ERK1/2. *Cell Signal* 19:1121–1131.
16. Durand RE (1982) Use of Hoechst-33342 for cell selection from multicell systems. *J Histochem Cytochem* 30:117–122.
17. Schofield CJ, Ratcliffe PJ (2004) Oxygen sensing by HIF hydroxylases. *Nat Rev Mol Cell Biol* 5:343–354.
18. Stern SA, Shah VM, Hardy BJ (1987) Structure-permeability Relationships in silicone polymers. *J Polym Sci Pol Phys* 25:1263–1298.
19. Helmlinger G, Yuan F, Dellian M, Jain RK (1997) Interstitial pH and pO(2) gradients in solid tumors in vivo: High-resolution measurements reveal a lack of correlation. *Nat Med* 3:177–182.
20. Carrilho E, Phillips ST, Vella SJ, Martinez AW, Whitesides GM (2009) Paper microzone plates. *Anal Chem* 81:5990–5998.
21. Frank R (1992) Spot-synthesis—an easy technique for the positionally addressable, parallel chemical synthesis on a membrane support. *Tetrahedron* 48:9217–9232.
22. Blackwell HE (2006) Hitting the SPOT: small-molecule macroarrays advance combinatorial synthesis. *Curr Opin Chem Biol* 10:203–212.
23. Bowman MD, O'Neill JC, Stringer JR, Blackwell HE (2007) Rapid identification of antibacterial agents effective against *Staphylococcus aureus* using small-molecule macroarrays. *Chem Biol* 14:351–357.
24. Kleinman HK et al. (1986) Basement-membrane complexes with biological-activity. *Biochemistry* 25:312–318.